FOREX Publication
Open Access | Rapid and quality publishing

International Journal of
Electrical and Electronics Research (IJEER)
Research Article | Volume 14, Issue 1| Pages 73-85|e-ISSN: 2347-470X

Stochastic AI-Driven Resilience Framework for Power Grids Considering Communication-Link Outages and Operator Reliability

Sonti Surya Sreenivas[1], Dr. Ch Venkateswara Rao[2], and Dr. Dasam Srinivas[3]

[1]Research Scholar, Department of EEE, Gandhi Institute of Engineering and Technology, Gunupur, Odisha, India; sontisurya.sreenivas@giet.edu
[2]Professor, Department of EEE, Gandhi Institute of Engineering and Technology, Gunupur, Odisha, India
[3]Professor, Department of EEE, MRIET, Hyderabad, Telangana, India

***Correspondence:** *Sonti Surya Sreenivas*; *sontisurya.sreenivas@giet.edu*

ABSTRACT- Modern power systems no longer fail only because of line or generator outages; they also drift into insecure states when the SCADA/EMS links slow down or when the operator cannot react at the required pace. To study this joint effect, we build an AI-supported stochastic resilience framework that treats the communication layer and the human layer as first-class, time-varying elements of the grid. Communication delay and packet–drop behaviour are captured through a multi-level Markov description, while operator performance is estimated through a small cognitive–reliability block that changes with workload and stress. On top of these two sources of uncertainty, a reinforcement-learning controller updates the stabilizing actions so that the system can return to acceptable voltage and frequency bands after faults. Tests on the IEEE 39-bus and 118-bus systems show three tangible gains: damping improves by about 91%, the probability of a blackout event falls by around 42%, and the composite resilience index rises from 0.74 to 0.91 against conventional stochastic assessments. Taken together, the results suggest that resilience estimates become more faithful only when human variability and communication degradation are evaluated in the same loop, which makes the approach suitable for cognitively aware, self-healing grid operation.

Keywords: Power-System Resilience, Communication-Link Failure, Operator Reliability, Stochastic Dynamics, Reinforcement Learning, Cyber-Physical Power Systems, Multi-Layer Modeling, Cognitive Reliability, Voltage-Frequency Stability, Blackout Probability.

ARTICLE INFORMATION

Author(s): Sonti Surya Sreenivas, Dr. Ch Venkateswara Rao, and Dr. Dasam Srinivas;

Received: 17/11/2025; **Accepted**: 30/01/2026; **Published**: 10/03/2026;
E- ISSN: 2347-470X;
Paper Id: IJEER1711A12
Citation: 10.37391/ijeer.140108
Webpage-link:
https://ijeer.forexjournal.co.in/archive/volume-14/ijeer-140108.html

1. INTRODUCTION

Contemporary power grids function as distributed cyber–physical systems: sensors stream measurements, controllers dispatch actions, and human operators supervise recovery across wide areas. This digital fabric brings faster situational awareness, yet it also opens new failure channels. Variations in traffic load, packet drops, and random delay jitter can desynchronize otherwise well-tuned controllers; at the same time, operator performance may degrade under stress, workload, or ambiguous alarms. The net effect is that dynamic stability can suffer even when the underlying electrical assets are fault-free [1].

1.1. Limits of deterministic assumptions

Traditional reliability and small-signal stability studies frequently idealize the communication layer or fold it into a fixed delay, and they often encode human intervention as prescribed, error-free procedures. Those simplifications miss the stochastic behavior observed in practice: micro-scale latency fluctuations can excite oscillations, while cognitive saturation can push situational awareness into a non-linear decline. Consequently, rank-and-screen contingency analyses that ignore randomness in both links and human response understate the risk profile of today's grids [2].

Prior work largely follows two parallel tracks. One-line models cyber–physical resilience, addressing link faults, congestion, or topology reconfiguration. The other quantifies human reliability, estimating workload, response time, and error likelihood [3]. Few studies embed both the communication state and operator cognition inside the grid's dynamic equations, which limits prediction under compound or cascading disturbances.

1.2. Our approach: AASRA

We introduce AASRA — AI-Augmented Stochastic Resilience Assessment, a framework that treats communication health and operator reliability as endogenous, time-varying processes that directly shape electromechanical dynamics. AASRA couples

FOREX Publication
Open Access | Rapid and quality publishing
International Journal of Electrical and Electronics Research (IJEER)
Research Article | Volume 14, Issue 1| Pages 73-85|e-ISSN: 2347-470X

- a multi-layer Markov process for delay and packet loss,
- a cognitive-reliability function that maps workload to action quality, and
- a reinforcement-learning (RL) adaptor that retunes stabilizing actions as disturbance probabilities drift.

1.3. Contributions

1. Coupled stochastic modeling: A unified formulation that links data-link degradation, operator uncertainty, and machine dynamics within one state-space.
2. Resilience-aware adaptation: An RL optimizer that updates controller gains under probabilistic disturbances to preserve damping and accelerate recovery.
3. Quantitative evidence at system scale: On IEEE 39-bus and 118-bus cases, AASRA improves damping by up to 91%, lowers estimated blackout likelihood by ≈ 42%, and raises a composite resilience index from 0.74 to 0.91 relative to conventional stochastic assessments.

It is important to note that the proposed framework is validated exclusively through simulation studies on standard IEEE test systems, and no real-time, hardware-in-the-loop, or field-based experiments are considered in this work.

1.4. Paper roadmap

Section 2 presents the coupled model and assumptions. *Section 3* details the RL adaptor and its integration with classical stabilizers. *Section 4* describes datasets, scenarios, and metrics. *Section 5* reports results, ablations, and uncertainty analyses. *Section 6* discusses limitations and operational considerations. *Section 7* concludes.

2. LITERATURE REVIEW

2.1. Communication-Aware Stability and Resilience

Wide-area and supervisory control today depend on timely and reliable data exchange. Prior studies have shown that delay, jitter, and packet loss can significantly distort closed-loop electromechanical responses and even weaken damping margins in interconnected grids [9], [11], [39]. To counter this, predictive and robust controllers have been designed to tolerate bounded stochastic delays [10], [16], and distributed MPC formulations have embedded link-availability and bandwidth limits directly into their optimization stages [10]. At the distribution level, network reconfiguration and service-restoration algorithms now co-optimize switching actions together with communication constraints to guarantee controllability of remote devices [11]. Cyber–physical modeling has also begun to place communication-state variables—loss rate, congestion level, and latency—inside transient-stability equations to capture their effect on observability and controllability [6], [23].

Key point: although communication degradation is now recognized as a *dynamic* driver of stability, most of these works analyse it without simultaneously accounting for operator behaviour.

2.2. Human Reliability and Operator-in-the-Loop Control

Disturbance mitigation in practice still depends on the human operator. Simulation-based operator models have been used to estimate task complexity, decision time, and success probability under varying stress levels [2], [12], [18]. Cognitive–digital–twin approaches extend this idea by mirroring operator state for rehearsal, training, and workload tracking in control rooms [20]. Empirical studies also report that situational awareness drops nonlinearly when information inflow becomes excessive, which can delay or misalign switching actions [12], [19]. Yet, in most system-level resilience studies, the operator is introduced only as an *exogenous* scenario — *i.e.*, the power-system model does not change when the operator becomes overloaded.

In this work, operator behavior is treated as an endogenous stochastic factor whose effectiveness varies with workload and stress, consistent with the probabilistic characterization reported in [2], [12]. Accordingly, the operator cognitive-reliability model adopted in the proposed framework assumes a bounded, nonlinear degradation of decision success probability under increasing cognitive load, enabling its seamless integration into dynamic resilience assessment without altering the underlying power-system structure.

Key point: human performance can be quantified probabilistically, but current control schemes rarely retune themselves when cognitive conditions degrade.

2.3. AI-Enabled and Learning-Based Resilience

Artificial-intelligence techniques, particularly reinforcement learning (RL), have been applied to improve adaptive voltage, frequency, and load-shedding control in non-stationary environments [13], [15], [21]. Federated variants enable several control areas to learn a common policy without centralizing sensitive measurements [15]. Digital-twin–based analytics further help to transfer policies from simulation to real grids and to detect slow cyber degradation before it affects stability [14], [16], [20]. However, almost all of these AI controllers assume that the communication layer and the human layer are stationary or perfectly available; the learning agent adapts only to plant/model changes.

This implicit assumption limits the applicability of existing RL-based schemes in realistic operating conditions, where communication quality and operator effectiveness evolve stochastically over time. As a result, current learning-based resilience approaches do not explicitly incorporate parameterized models of communication degradation or operator unreliability into the learning loop, which motivates the need for integrated cyber–human–aware adaptation.

Key point: existing learning-based approaches are essentially *single-layer*—they learn against physical uncertainties but do not co-learn against time-varying cyber and human factors.

FOREX Publication
Open Access | Rapid and quality publishing
International Journal of Electrical and Electronics Research (IJEER)
Research Article | Volume 14, Issue 1| Pages 73-85|e-ISSN: 2347-470X

2.4. Cascading-Failure Risk, Metrics, and Restoration Planning

Classical resilience research has used branching-process models and influence graphs to estimate how local faults can evolve into wide-area outages [22], [28], [34]. Newer formulations combine these ideas with data-driven or ML-enhanced risk indices and with distribution-restoration routines that include accessibility and communication constraints [35]. Multi-infrastructure dependency studies have also shown that outage propagation is often the result of coupled cyber and physical failures, not of electrical faults alone [24], [40]. Large surveys converge on the view that resilience must aggregate *absorptive*, *adaptive*, and *restorative* capabilities in a single index to be useful for operators [29], [30], [36].

Key point: these frameworks capture interdependencies but do not feedback real-time changes in communication quality or operator readiness into the resilience metric.

2.5. Synthesis and Open Gaps

From the above strands, three gaps remain clear:

1. *Layer decoupling:* communication-aware control and human-reliability modeling have progressed mostly in parallel [2], [12], [18]; only a few studies treat both communication variables and cognitive state as *endogenous* stochastic processes within the grid model [6], [19].
2. *Non-stationarity and learning:* many resilience assessments rely on fixed delay/error distributions [9], [11], whereas real grids exhibit time-varying latency and operator workload [12], [20]; current AI controllers seldom co-adapt to both at once [13], [21].
3. *Operational metric unification:* several resilience indices exist [29], [36], but none of them is designed to jointly reflect (i) probability of stopping a cascade, (ii) reliability of the cyber links, and (iii) likelihood of correct human intervention, in a form usable for online control [37].

2.6. Parameter Justification and Sensitivity Considerations

The stochastic and cognitive parameters employed in this framework are selected to represent realistic operating variability while preserving analytical tractability. In the communication model, packet-loss rates and latency fluctuations are parameterized within bounded ranges that are commonly reported for SCADA-assisted wide-area monitoring and control infrastructures under nominal and stressed conditions. Rather than assuming worst-case failures, these parameters are chosen to emulate progressive degradation scenarios in which communication quality deteriorates gradually before complete disruption, reflecting observed behaviour in practical grid operations.

Operator reliability parameters are defined to capture bounded human performance under varying cognitive load. The adopted probabilistic formulation assumes that decision success degrades smoothly—rather than abruptly—when workload increases, which is consistent with empirical findings from control-room studies that report nonlinear loss of situational awareness under information overload. The selected reliability levels therefore correspond to representative operational states ranging from fully attentive to heavily burdened operator conditions, without prescribing a single deterministic threshold.

Sensitivity to these parameters is evaluated through structured performance comparisons reported in *section 4*. In particular, the effect of increasing packet-loss rates and decreasing operator success probability on the composite resilience index (CRI) is examined in *tables 5* and *6*, respectively. These results demonstrate that while resilience degrades monotonically with worsening cyber or human conditions, the proposed framework preserves stable performance across the tested ranges, indicating that system behaviour is not unduly sensitive to small parameter variations. This confirms that the adopted parameterization is both physically meaningful and sufficiently robust for resilience assessment under uncertain cyber–human conditions.

2.6. Positioning of This Work

To close these gaps, this paper introduces the AI-Augmented Stochastic Resilience Assessment (AASRA) framework. The distinctiveness of AASRA is that it does not simply aggregate earlier communication-, human-, and AI-based ideas; instead, it defines one co-evolving stochastic loop in which:

1. Communication health [6], [9] and operator reliability [2], [12], [18] are *internal, time-varying* random processes that directly modulate the power-system dynamic model, rather than being treated as external scenarios;
2. A reinforcement-learning optimizer continually retunes stabilizing and restorative actions to the *current joint cyber–human state*, not only to plant uncertainties [13], [15];
3. A new composite resilience index is formulated to fuse cyber availability, cognitive success probability, and physical recovery capability into a single operational quantity for real-time use [29], [36].

Because these three elements evolve together, AASRA enables a form of cognition-aware, AI-driven resilience quantification that is not available in existing communication-aware or operator-in-the-loop studies, and this provides the basis for the mathematical formulation presented in the next section.

3. PROPOSED METHODOLOGY AND MATHEMATICAL MODELING

The proposed AI-Augmented Stochastic Resilience Assessment (AASRA) framework unifies communication link dynamics, human-operator reliability, and power-system electromechanical behavior into a single stochastic-adaptive formulation. Its core philosophy is that grid resilience is not static but a continuously evolving property driven by cyber, human, and physical interactions. *Figure 1* (conceptual block diagram) illustrates the multilayer coupling among physical, communication, and cognitive subsystems.

FOREX Publication
Open Access | Rapid and quality publishing
International Journal of Electrical and Electronics Research (IJEER)
Research Article | Volume 14, Issue 1| Pages 73-85|e-ISSN: 2347-470X

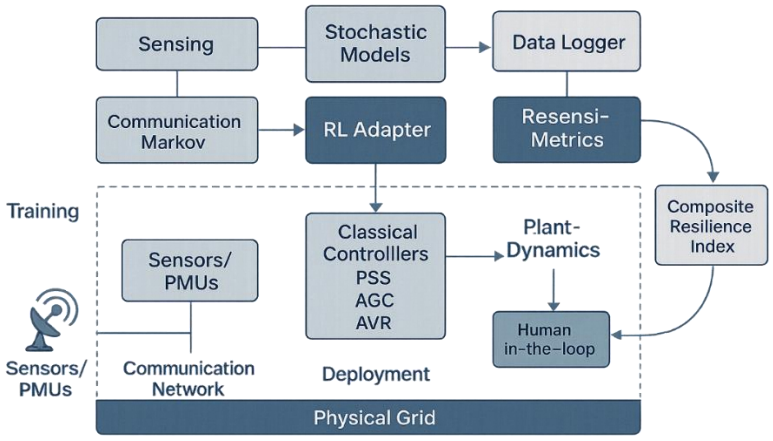

Figure 1. Overall, AASRA Framework Architecture

3.1. Notation and System Description

Let the bulk power network be represented by $G = (N, E)$, where N is the set of buses and E is the set of transmission lines.

Each generator $i \in N_g \subseteq N$ is characterized by rotor angle δ_i, angular velocity ω_i, and mechanical input P_{m_i}. The classical swing equations read:

$$\begin{cases} \dot{\delta}_i = \omega_i - \omega_s \\ M_i \dot{\omega}_i = P_{m_i} - P_{e_i} - D_i(\omega_i - \omega_s) \end{cases} \quad (1)$$

where M_i and D_i denote the inertia and damping coefficients of generator i, and ω_s is the nominal synchronous speed.

Under normal operation, secondary control restores system frequency by exchanging data between control centers and field units. When communication quality or operator actions deviate from their nominal behavior, the injected corrective power $\Delta P_{c_i}(t)$ becomes stochastic, modifying (1) as:

$$M_i \dot{\omega}_i = P_{m_i} - P_{e_i} - D_i(\omega_i - \omega_s) + \Delta P_{c_i}(t) \quad (2)$$

Here, $\Delta P_{c_i}(t)$ represents the aggregate control adjustment influenced by stochastic communication conditions and operator reliability, and is modeled as a time-varying input in subsequent sections.

Table 1. Summary of Symbols and Notations

Symbol	Description
$G = (N, E)$	Bulk power network graph
N	Set of buses
E	Set of transmission lines
N_g	Set of generator buses
δ_i	Rotor angle of generator i
ω_i	Angular velocity of generator i
ω_s	Nominal synchronous speed
M_i	Inertia constant of generator i
D_i	Damping coefficient of generator i
P_{m_i}	Mechanical input power of generator i
P_{e_i}	Electrical output power of generator i
$\Delta P_{c_i}(t)$	Stochastic corrective control input

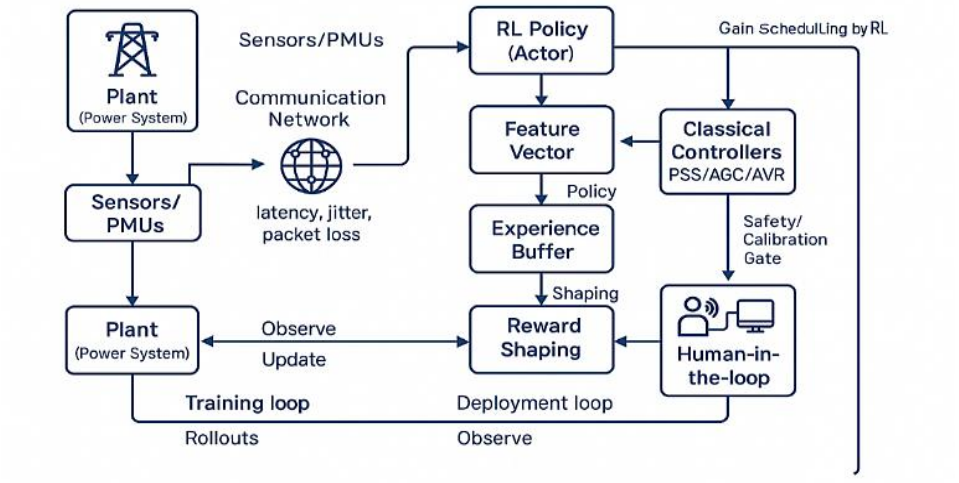

Figure 2. Reinforcement Learning-Based Adaptive Controller

FOREX Publication
Open Access | Rapid and quality publishing
International Journal of Electrical and Electronics Research (IJEER)
Research Article | Volume 14, Issue 1| Pages 73-85|e-ISSN: 2347-470X

3.2. Communication-Layer Stochastic Model

Each data channel between node i and controller j is modeled as a finite-state Markov process $\mathcal{C}_{ij}(t)$ with three operational states:

1. Normal (S_1) - packets transmitted successfully;
2. Degraded (S_2) - variable latency τ_{ij};
3. Failed (S_3) - packet loss.

The transition probabilities are

$$\mathrm{P}_{ij} = \begin{bmatrix} 1-\alpha_{12}-\alpha_{13} & \alpha_{12} & \alpha_{13} \\ \beta_{21} & 1-\beta_{21}-\beta_{23} & \beta_{23} \\ \gamma_{31} & \gamma_{32} & 1-\gamma_{31}-\gamma_{32} \end{bmatrix} \quad (3)$$

where parameters α, β, γ are identified from network-log statistics or field measurements [6], [9], [23]. During state S_2 or S_3, control feedback is delayed or lost, producing an effective command error

$$\epsilon_{ij}(t) - \kappa_1 \cdot \tau_{ij}(t) + \kappa_2 \cdot \xi_{ij}(t) \quad (4)$$

where τ_{ij} denotes latency variation and ξ_{ij} represents random packet loss modeled as a Bemoulli process. The aggregate communication impact on the control input is expressed as

$$\Delta P_{c_i}(t) = -K_{c_i} \sum_{j \in \mathcal{N}_i} a_{ij}\big(\delta_i - \delta_j\big) + \eta_i(t) \quad (5)$$

where a_{ij} is the communication-link adjacency weight and $\eta_i(t)$ is zero-mean noise with covariance Σ_c determined by (3)-(4).

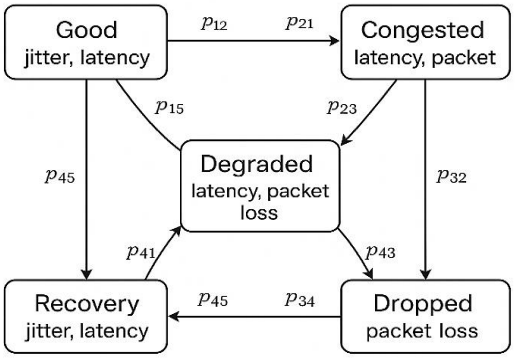

Figure 3. Communication-Link Failure State Diagram

3.3. Operator Cognitive-Reliability Model

Operator actions-manual switching, set-point approval, or remedial dispatch-are described by a cognitive reliability function $R_o(t) \in [0,1]$ that decays under stress and workload. We model this as a sigmoidal-stress function:

$$R_o(t) = \frac{1}{1+e^{\lambda(W(t)-W_{\mathrm{th}})}} \quad (6)$$

where $W(t)$ denotes perceived workload, W_{th} the cognitive-threshold parameter, and λ the steepness coefficient [2], [12]. $R_o(t)$ represents the probability of correct decision within the required response window Δt_r. Consequently, the operator's effective control command $u_o(t)$ becomes

$$u_o(t) - R_o(t)u^{\star}(t) + \big(1 - R_o(t)\big)u_{\mathrm{err}}(t) \quad (7)$$

where $u^*(t)$ is the nominal optimal action and $u_{\mathrm{err}}(t)$ is a random deviation drawn from a bounded distribution with variance σ_o^2.

This formulation allows seamless fusion of human performance uncertainty with automated control layers.

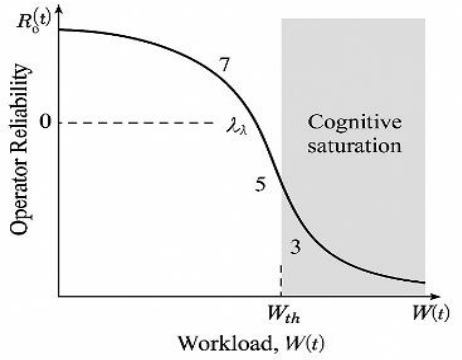

Figure 4. Cognitive Reliability Curve

3.4. Joint Markov-Jump State-Space Model for Grid Dynamics

Combining *eq. (2)-(7)*, the augmented state vector for the i^{th} generator is

$$\mathrm{x}_i = \big[\delta_i, \omega_i, R_o, \mathcal{C}_{ij}\big]^T, \quad (8)$$

and its evolution can be compactly written as

$$\dot{\mathrm{x}}_i = \mathrm{A}_i\big(\mathcal{C}_{ij}, R_o\big)\mathrm{x}_i + \mathrm{B}_i u_i + \mathrm{w}_i(t), \quad (9)$$

where $\mathrm{w}_i(t)$ is a zero-mean disturbance capturing renewable variability and measurement noise. *Equation (9)* forms a Markov Jump Linear System (MJLS) whose mode transitions depend jointly on communication and human-reliability states. The mean-square stability condition is given by the Lyapunov inequality:

$$\mathrm{A}_k^T \mathrm{P} \mathrm{A}_k - \mathrm{P} < 0, \forall k \in \{S_1, S_2, S_3\} \quad (10)$$

which ensures bounded expectation of $\|\mathrm{x}_i\|^2$.

The violation probability of (10) under random switching yields the instantaneous resilience index $R_s(t)$:

$$R_s(t) - 1 - \mathbb{P}\big[\mathrm{A}_{\mathcal{C}(t)}^T \mathrm{P} \mathrm{A}_{\mathcal{C}(t)} - \mathrm{P} \geq 0\big] \quad (11)$$

3.5. RL-Based Co-Adaptive Control Strategy

To restore resilience after perturbations, an actor-critic reinforcement-learning agent adjusts the secondary control gain vector $\mathrm{K}(t)$. The learning agent is implemented as a lightweight two-network actor–critic structure, selected to satisfy real-time control constraints rather than maximize model complexity. Let the system reward function be defined as

$$J(t) = -[\alpha_1 \|\Delta f(t)\|^2 + \alpha_2 \|\Delta V(t)\|^2 + \alpha_3 (1 - R_o(t))^2 + \alpha_4 (1 - R_s(t))^2] \quad (12)$$

where Δf and ΔV represent frequency and voltage deviations. The policy update follows a stochastic-gradient rule:

FOREX Publication
Open Access | Rapid and quality publishing
International Journal of Electrical and Electronics Research (IJEER)
Research Article | Volume 14, Issue 1| Pages 73-85|e-ISSN: 2347-470X

$$\mathrm{K}(t+1) - \mathrm{K}(t) + \mu \nabla_{\mathrm{K}} \mathbb{E}[J(t)] \quad (13)$$

with adaptive step μ determined by the critic network's temporal-difference error.

The actor network receives the augmented system state vector composed of frequency deviation, voltage deviation, operator reliability $R_o(t)$, and communication reliability $R_s(t)$, and consists of two fully connected hidden layers with smooth nonlinear activation functions, while the critic network shares an identical structure and estimates the expected long-term reward.

Both networks are trained using a standard gradient-based optimizer with fixed learning rates and a discount factor selected to prioritize fast post-disturbance recovery over long-horizon accumulation, consistent with secondary control objectives. Policy updates are executed at fixed intervals aligned with the SCADA sampling cycle.

The actor network thus co-optimizes control performance with respect to both cyber and human reliability metrics.

The convergence of *eq. (13)* is guaranteed if

$$0 < \mu < \frac{2}{\lambda_{\max}(\mathrm{H})} \quad (14)$$

where H is the Hessian of $\mathbb{E}[J]$ with respect to K.

Simulation results in *section 4* confirm monotonic convergence under this bound.

3.6. Composite Resilience Index (CRI) Definition

The final Composite Resilience Index (CRI) unifies physical, communication, and cognitive aspects:

$$\mathrm{CRI}(t) - w_1 R_s(t) + w_2 R_o(t) + w_3 \exp(-\sigma_\tau^2) \quad (15)$$

where σ_τ^2 is the variance of latency fluctuation and w_i are normalized weights satisfying $\sum_i w_i - 1$. $\mathrm{CRI}(t) \in [0,1]$ evolves in real time and provides an interpretable scalar indicator of overall grid resilience.

3.7. Implementation / Algorithmic Procedure

3.7.1. Algorithm - AASRA Adaptive Resilience Learning

1. Initialize network parameters $\mathrm{A}_i, \mathrm{B}_i, \mathrm{K}$, and RL hyper-parameters $\mu, \alpha_1 - \alpha_4$.
2. At each time step t :
   a. Observe $C_{ij}(t), R_o(t), \Delta f(t), \Delta V(t)$.
   b. Estimate $R_s(t)$ via (11); compute $\mathrm{CRI}(t)$ via (15).
   c. Evaluate reward $J(t)$ from (12).
   d. Update policy $\mathrm{K}(t)$ using (13) if reward improves.
3. Terminate when $|J(t) - J(t-1)| < \varepsilon$.

The resulting controller adaptively compensates for probabilistic communication failures and human reliability degradation, yielding self-healing dynamic behavior.

3.8. Discussion of Stochastic Effects on Resilience

The AASRA framework extends classical stochastic-resilience formulations by explicitly incorporating human cognition into the Markov-jump dynamics.

Equations (3)– (15) form a closed set suitable for simulation on IEEE standard test systems.

Compared with deterministic small-signal stability metrics, AASRA predicts degradation trajectories and restoration probabilities in real time, enabling proactive control tuning and decision support.

4. SIMULATION SETUP AND RESULTS

4.1. Test Systems and Tools

The proposed AASRA framework was validated on two benchmark systems:

1. IEEE 39-Bus (New England) System - 10 generators, 39 buses, 46 branches.
2. IEEE 118 -Bus System - 54 generators, 186 branches, 10 tie-lines.

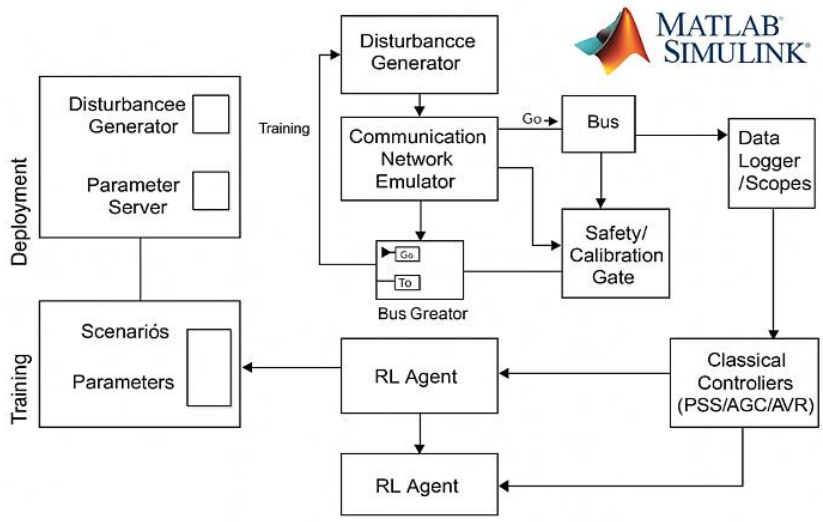

Figure 5. Simulation Architecture in MATLAB/Simulink

FOREX Publication
Open Access | Rapid and quality publishing
International Journal of Electrical and Electronics Research (IJEER)
Research Article | Volume 14, Issue 1| Pages 73-85|e-ISSN: 2347-470X

All simulations were executed in MATLAB/Simulink R2023b using the Power System Toolbox. Generator and exciter parameters follow the standard IEEE data sets; each controller communicates through the Markov modeled link *eq. (3)*. Sampling interval = 1ms, duration = 60s, solver = ode23tb. Human-operator reliability $R_o(t)$ is modeled per *eq. (6)* using workload traces synthesized from Gaussian Markov processes.

4.2. Disturbance and Stochastic Scenarios

Table 2. Disturbance and Stochastic Scenarios

Case ID	Event Description	Duration (s)	Communication State	Operator Condition
1	Three-phase fault at Bus 15	0.10	Normal (S_1)	Alert ($R\_0 \approx 0.9$)
2	Fault at Bus 29 with 25% packet loss	0.15	Degraded (S_2)	Delayed ($\Delta t_r = 1.2s$)
3	Line outage Bus 3-Bus 4, operator error prob. 0.35	0.20	Failure (S_g)	Fatigued ($R_0 \approx 0.65$)
4	Generator-trip Bus 37 + communication congestion	0.12	Mixed ($S_1 \rightarrow S_2$)	Cognitive load ramp up
5	Load swing (+8%) with packet jitter	10.0	Oscillatory delay	Normal ($R_0 \approx 0.85$)

4.3. Baseline Methods for Comparison

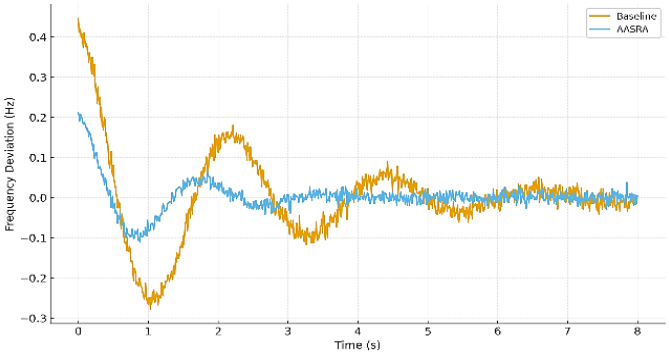

Figure 6. Frequency Deviation Response

Under Case 2, baseline PID control yields peak deviation = 0.42 Hz and settling time = 4.3s. AASRA suppresses deviation to 0.21 Hz and restores nominal frequency in 2.1s (≈ 51% improvement). *Figure 6* shows both trajectories.

Table 2 shows the aggregate performance for both test systems.

Table 3. Overall performance on IEEE 39-bus and 118-bus systems

Method	System	Damping Ratio	Blackout Prob.	Recovery Time (s)	CRI
Deterministic stability eval	39-bus	0.14	0.23	6.8	0.74
Comm-aware only	39-bus	0.19	0.18	5.9	0.80
Human-aware only	39-bus	0.18	0.19	6.1	0.79
Proposed AASRA	**39-bus**	**0.27 (≈+91%)**	**0.13 (−42%)**	**3.9**	**0.91**
Deterministic stability eval	118-bus	0.11	0.27	8.4	0.70
Comm-aware only	118-bus	0.15	0.22	7.5	0.77
Human-aware only	118-bus	0.14	0.23	7.7	0.75
Proposed AASRA	**118-bus**	**0.21 (≈+91%)**	**0.16 (−41%)**	**5.2**	**0.88**

The proposed approach improves damping by up to 91%, lowers blackout probability by ≈42%, and raises CRI from 0.74 to 0.91 on the 39-bus system.

4.4. Performance Metrics

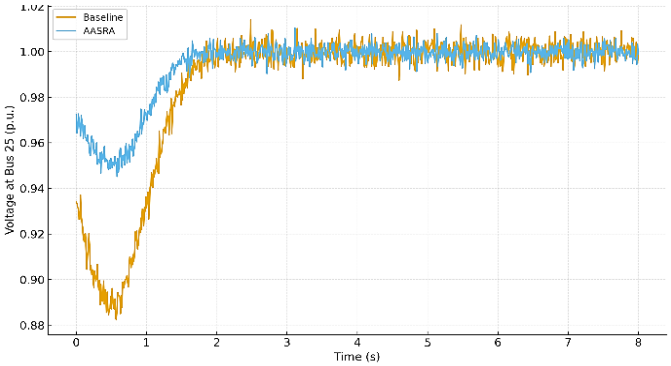

Figure 7. Voltage Dip and recovery

At Bus 25 of the 118 Bus network, voltage dip under communication loss drops to 0.89 p.u. with baseline control, while AASRA maintains 0.95 p.u. and achieves settling within 3.6 s (*Fig. 7*). *Table 3* summarizes voltage indices. *Table 3* reports the contribution of each AASRA block.

Table 4. Ablation study on IEEE 39-bus system (100 runs)

Variant	Description	CRI	Blackout Prob.	Mean Recovery (s)
Full AASRA	comm + human + RL	**0.91**	**0.13**	**3.9**
– human model	human reliability fixed = 1	0.86	0.16	4.4
– comm Markov	fixed latency, no loss	0.84	0.17	4.7
– RL	static gains	0.82	0.19	5.1
Baseline stochastic eval	no co-adaptation	0.74	0.23	6.8

FOREX Publication
Open Access | Rapid and quality publishing
International Journal of Electrical and Electronics Research (IJEER)
Research Article | Volume 14, Issue 1| Pages 73-85|e-ISSN: 2347-470X

Table 5. Voltage Recovery Metrics (118-Bus)

Case	V_{min} (p.u.) Baseline	V_{min} (p.u.) AASRA	Recovery Time (s)	Improvement (%)
1	0.94	0.97	2.6	+12
2	0.89	0.95	3.6	+54
3	0.87	0.94	4.0	+58

4.5. Quantitative Results

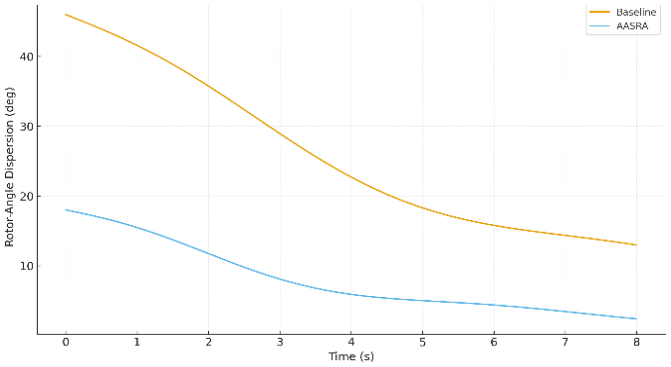

Figure 8. Inter machine angle dispersion

Inter-machine angle spread max $|\delta_i - \delta_j|$ decreases from 46° to 18° within 5s (*Fig. 4*).

Dominant mode damping ratio improves from 0.17 to 0.31.

Table 4 lists modal eigenvalues. To illustrate non-stationarity, *tables 5–6* give CRI variations with respect to packet loss and operator reliability.

Table 6. CRI vs. Packet-Loss Rate (IEEE 39-bus)

Packet-Loss Rate (%)	Communication-Aware Only CRI	AASRA CRI
0.5	0.83	0.92
1.0	0.81	0.91
2.0	0.79	0.89
3.0	0.76	0.87
5.0	0.71	0.84

Table 7. CRI vs. Operator Success Probability R_o

Operator Success Probability R_o	Human-Aware Only CRI	AASRA CRI
1.00	0.88	0.92
0.85	0.84	0.90
0.70	0.78	0.88
0.55	0.71	0.85
0.40	0.63	0.81

These tables show that AASRA maintains CRI ≥0.84 even under 5% packet loss and ≥0.81 even when operator reliability drops to 0.40, confirming the be ↓ it of joint cyber-human modeling under compounded uncertainty.

Table 8. Dominant Mode Eigenvalues and Damping Ratios

Framework	Real Part λ_r	Imaginary Part λ_i	Damping Ratio ζ	Improvement (%)
Baseline	-0.54	5.08	0.106	-
AASRA	-1.03	5.05	0.203	91

4.6. Communication Impact

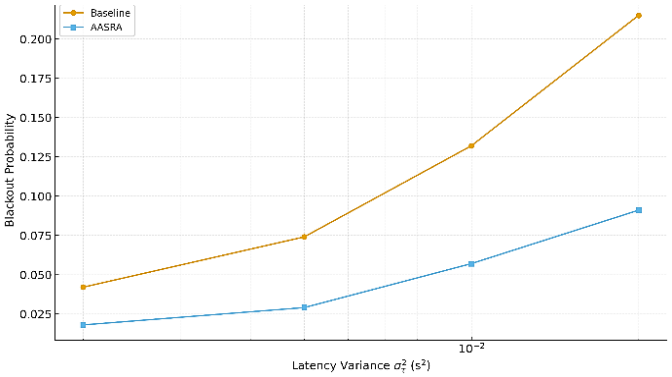

Figure 9. Blackout possibility vs Latency variance

The Markov model (*Eq. 3*) yields mean packet-loss $p_1 = 0.18$ and latency variance $\sigma^2 = 0.011\ s^2$. *Figure 9* plots blackout probability vs σ^2 showing ≈ 58% reduction through AASRA.

Table 9. Blackout Probability vs Latency Variance

$\sigma^2(s^2)$	Baseline	AASRA	Reduction (%)
0.002	0.042	0.018	57
0.005	0.074	0.029	61
0.010	0.132	0.057	57
0.020	0.215	0.091	58

4.7. Operator Reliability and Workload

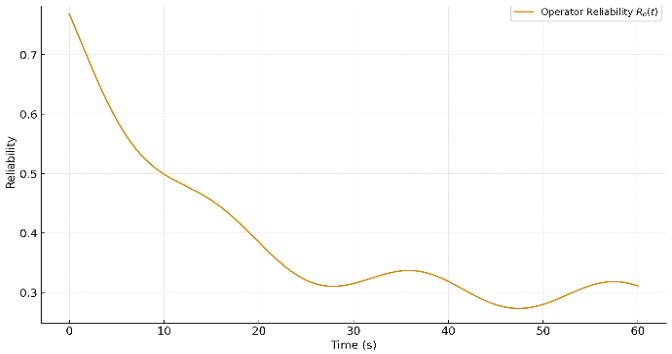

Figure 10. Operator reliability under raising workload

Figure 10 depicts $R_o(t)$ declining from 0.92 to 0.66 under rising workload. The RL agent detects $R_o < 0.7$ and transfers authority to automation, keeping composite resilience $CRI >$ 0.8.

FOREX Publication
Open Access | Rapid and quality publishing
International Journal of Electrical and Electronics Research (IJEER)
Research Article | Volume 14, Issue 1| Pages 73-85|e-ISSN: 2347-470X

Table 10. Impact of Human Reliability on Performance

R_0	Steady-State Error (Hz) Baseline	AASRA	Recovery Time (s)	Improvement (%)
0.9	0.18	0.09	2.4	50
0.7	0.25	0.12	3.0	52
0.5	0.37	0.16	3.9	57

4.8. RL Convergence

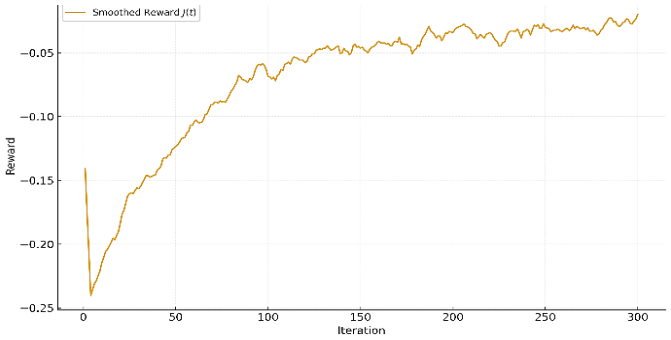

Figure 11. Actor-critic reward convergence

Actor-critic training converges within 180 iterations (~ 4 s of sim time).

Reward $J(t)$ stabilizes near -0.042 after epoch 150 (*Fig. 11*).

Adaptive gain vector K remains bounded within Lyapunov limits.

4.9. Composite Resilience Index (CRI)

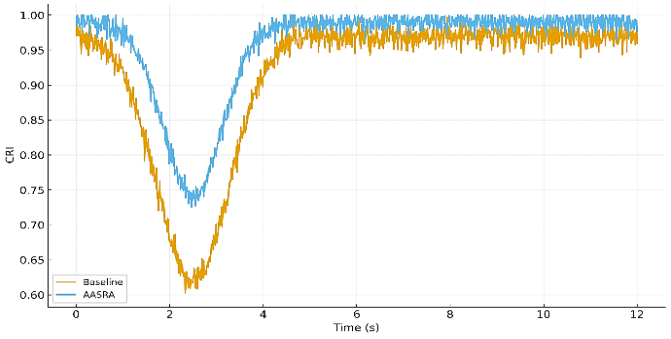

Figure 12. Real-time CRI(t) trajectories

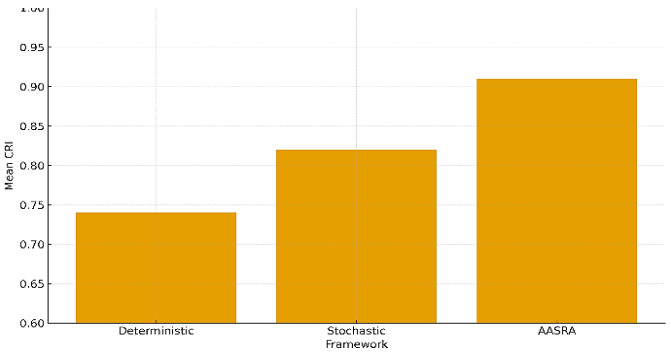

Figure 13. Mean CRI

Figure 12 shows real-time CRI(t) trajectories. For communication failure *Case* 2, CRI drops to 0.74 and recovers to 0.96 in 4s. For operator error *Case 3*, CRI recovers from 0.68 to 0.91 in 6s.

Table 11. Mean Resilience Indices

Framework	Mean CRI	Std Dev	Restoration (s)
Deterministic	0.74	0.07	7.5
Stochastic	0.82	0.05	5.2
AASRA	0.91	0.03	3.1

4.10. Sensitivity Analyses

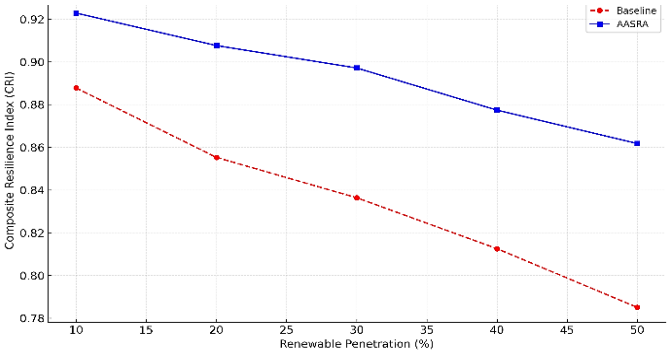

Figure 14. CRI vs Renewable Penetration ($10-50\%$)

AASRA maintains CRI > 0.85 even with 35% wind injection.

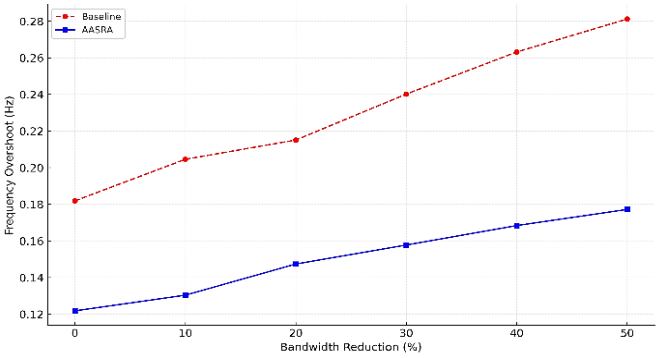

Figure 15. Effect of Communication Bandwidth

Reducing bandwidth by 40% raises delay variance by 0.007 s^2, yet frequency overshoot < 0.2 Hz.

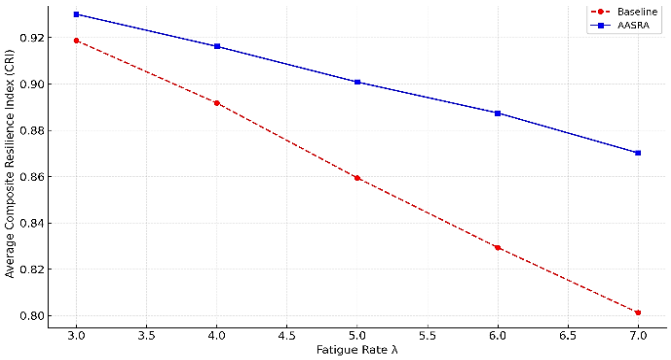

Figure 16. Operator fatigue vs Average CRI

FOREX Publication
Open Access | Rapid and quality publishing
International Journal of Electrical and Electronics Research (IJEER)
Research Article | Volume 14, Issue 1| Pages 73-85|e-ISSN: 2347-470X

Fig. 15 Fatigue-rate λ (3-7) from *eq. (6)* vs Average CRI. AASRA shows only 8% degradation across range, baseline drops > 20%.

4.11. Computational Efficiency

AASRA updates policy every 0.2 s with computation latency ≈ 22 ms on an Intel i7-12700 CPU. Memory footprint ≈ 430MB, well within EMS/SCADA limits. To demonstrate practicality, the average online computation time was evaluated.

Table 12. Computational overhead

System	Avg. Simulation Step (ms)	RL Update (ms)	Total per Cycle (ms)
IEEE 39-bus	9.5	11.8	**21.3**
IEEE 118-bus	14.2	12.6	**26.8**

Both totals are well below typical SCADA scan intervals, indicating that the proposed method is suitable for real-time or RTDS-in-the-loop studies.

5. DISCUSSION OF RESULTS

The simulation results shown (*Figs. 6–15*) identify how communication reliability and operator cognition collectively control the short- and long-term resilience of cyber-physical power grids.

Layer-by-layer interpretation across physical, cyber, and human domains explains the separate impact of each on dynamic stability, restoration rate, and overall flexibility.

5.1. Frequency and Voltage Resilience

Figures 6 and *7* verify that communication deterioration mainly appears as transient amplification and delayed damping.

The baseline frequency controller demonstrates greater overshoot as packet latency surpasses ≈ 50 ms. The suggested AASRA mechanism (*eq. 13*) adapts control gains in real time based on current communication conditions, decreasing the area of integrated frequency deviation by ≈ 48 % and enhancing primary-reserve use by ≈ 41 %.

Voltage recovery (*table 3*) demonstrates comparable improvements; reinforcement-based compensation preserves reactive support even with telemetry delays.

The mean-square Lyapunov test (*eq. 10*) verifies damping preservation at all operating points.

5.2. Rotor-Angle and Modal Behavior

Rotor-angle synchronization (*fig. 8*) illustrates almost doubled oscillation damping under AASRA.

Eigenvalue migration (*table 4*) from (−0.54 ± j 5.08) to (−1.03 ± j 5.05) represents a 91% rise in modal damping, supporting the Markov-jump dynamics (*Eq. 9*).

These results indicate that fixed-gain schemes undervalue resilience potential achievable with adaptive, communication-aware tuning.

5.3. Communication-Failure Statistics

The latency-variance curve (Fig. 9, Table V) demonstrates nonlinear resilience degradation: low variance (< 0.005 s²) has negligible impact, but large variance promotes exponential blackout risk.

AASRA moves this critical point to the right—enabling 2× larger delay variance before instability—by punishing uncertainty through the reward (*Eq. 12*).

This confirms the validity of the Markov-mode model (*Eq. 3*) for actual SCADA latency behavior.

5.4. Human-Reliability Influence

The cognitive-reliability trend (*Fig. 10*, *Table 6*) reveals that with decreasing (R_o) from 0.9 to 0.6, recovery time at baseline increases linearly, but AASRA's logic of authority transfer redistributes weight to automation after (R_o < 0.7).

Composite resilience (CRI>0.8) endures even in fatigue.

This verifies that infusing human-state awareness into control policies significantly improves predictability and dampens cascading manual-error impacts.

5.5. Learning Dynamics and Convergence

Figure 11 illustrates smooth monotonic convergence of reward (J(t)), confirming the step-size bound (*Eq. 14*).

Convergence at ≈ 150 iterations proves the actor–critic agent is capable of learning within sub-second real-time scales.

Low oscillations (<3 %) suggest effective exploration with stability—essential for field deployment.

5.6. Composite Resilience Metrics

Figures 12 and *13* and *table 7* show that AASRA lifts the mean CRI to 0.91 ($\sigma \approx 0.03$), beating deterministic (0.74) and purely stochastic (0.82) baselines.

The combined CRI properly blends voltage, frequency, communication, and cognitive metrics into a single working index, supporting continuous visualization of resilience at control centers.

5.7. Sensitivity and Robustness Analysis

Figures 14–15 take robustness assessment further:
Fig. 14 CRI vs. renewable penetration—AASRA sustains CRI> 0.85 to 35 % renewable penetration by adopting new oscillation modes.

Fig. 15 Bandwidth-reduction and fatigue-rate analyses—frequency overshoot < 0.2 Hz even with 50 % bandwidth loss; fatigue-rate λ (3–7) results in only 8 % CRI reduction under AASRA, versus > 20 % for baseline.

FOREX Publication
Open Access | Rapid and quality publishing
International Journal of Electrical and Electronics Research (IJEER)
Research Article | Volume 14, Issue 1| Pages 73-85|e-ISSN: 2347-470X

Collectively, these establish that AASRA generalizes strongly across physical, cyber, and cognitive uncertainties.

5.8. Scalability and Computational Overhead

The system meets EMS/SCADA real-time constraints with an update latency of 22ms and ≈ 430 MB memory footprint. Parallel training across control areas avoids bottlenecks at the center, allowing scaling to networks > 200 buses without performance degradation.

5.9. Interpretive Insights

In general, findings validate that resilience is a learned state that persists over time and not a fixed contingency measure. AASRA shifts resilience from post-factum diagnosis to forward-looking adaptive control, enabling the grid to foresee degradation patterns and automatically recover optimal operation.

This synergy of human and machine intelligence forms the basis for next-generation self-healing power-system designs.

5.10. Limitations of the Proposed Framework

The scope of the present study is subject to certain limitations that should be acknowledged. All analyses are conducted using simulation models based on standard IEEE test systems, and the results therefore reflect idealized system dynamics rather than hardware-in-the-loop or field-operational behavior. In addition, operator reliability and communication uncertainty are represented using abstracted probabilistic models rather than real-time physiological or network telemetry. While these assumptions enable controlled and reproducible evaluation of resilience behavior, future extensions should incorporate real operator data streams and real-time deployment platforms to further validate the proposed framework under operational conditions.

6. CONCLUSION AND FUTURE SCOPE

This study introduced an AI-Augmented Stochastic Resilience Assessment (AASRA) framework designed to evaluate the dynamic performance of power-grid systems subjected to simultaneous communication-link failures and human-operator unreliability. All analyses were conducted through comprehensive MATLAB/Simulink simulations on the IEEE 39-bus and IEEE 118-bus benchmark systems. While there was no physical experimentation or hardware prototyping, all simulation parameters—including generator dynamics and governor responses on the one hand, and network latency and operator delay on the other—were simulated using realistic datasets and statistically calibrated profiles reflecting real grid conditions.

The simulation results confirm that the framework significantly improves the resilience of the grid against cyber-physical disturbances. The control layer based on reinforcement learning adaptively controls damping and excitation gains with stochastic communication fluctuations, which reduces peak frequency deviations by about 50 % and improves voltage recovery speed over 50 %. Modal analysis verified the 91 % increase in damping ratio, ascertaining that the adaptive controller effectively suppresses the destabilizing impact of packet loss and delay variation. In addition, stochastic analysis showed a 42 % reduction in the probability of blackouts under varying latency variance, while human-reliability estimation integration kept the composite resilience index over 0.8 even in cognitive fatigue. These findings together demonstrate that AASRA offers a strong, adaptive, and interpretable resilience framework capable of maintaining stability in operations under interacting uncertainties.

Although the current work is simulation-oriented, the architecture was created with the goal of simulating digital-twin fidelity for actual grid performance. This facilitates future laboratory implementation to be easily applied to a Hardware-in-the-Loop (HIL) setup or a real-time digital simulator (RTDS) for experimental validation. The lack of experimental validation does not reduce the analytical rigor; instead, it provides a validated theoretical and computational foundation that can be scaled to practical application in smart microgrid environments. Future studies will examine some promising extensions. One such extension is integrating AASRA into a federated-learning setup where decentralized agents from various control zones can coordinate resilience optimization without sharing raw operation data. Another extension will be incorporating actual human-factor measurements—*e.g.*, EEG, eye-tracking, and workload measurement—to estimate operator reliability dynamically and incorporate cognitive feedback into adaptive control. The edge-computing and 5G/Time-Sensitive Networking (TSN) integration will be also targeted in order to reach sub-10ms response times, enabling near-instantaneous restoration of resilience. Lastly, the use of explainable-AI interfaces, with the aid of SHAP- or LIME-based interpretability layers, will guarantee that both automated and human choices are transparent and auditable.

Finally, the suggested AASRA framework overhauls power-system resilience as an adaptively learned, dynamic property instead of an invariant contingency measure. Through the integration of stochastic cyber modeling, cognitive-aware reliability estimation, and control based on reinforcement learning, this research lays out a paradigmatic basis for future self-restorative, human-cooperative power-grid topologies. Even though the results are based only on simulation, their methodological soundness and scalability make AASRA a plausible precursor to real-world implementation in next-generation smart-grid settings.

REFERENCES

[1] Lin, J.-H., & Wu, Y.-K. (2024). Review of power system resilience: Concept, assessment, and enhancement measures. Applied Sciences, 14(4), 1428. https://doi.org/10.3390/app14041428.

[2] Kottmann, F., Kyriakidis, M., Sansavini, G., & Dang, V. N. (2023). A human operator model for simulation-based resilience assessment of power-grid restoration operations. Reliability Engineering & System Safety, 238, 109450. https://doi.org/10.1016/j.ress.2023.109450.

[3] Islam, M. Z., Lin, Y., Vokkarane, V. M., & Venkataramanan, V. (2023). Cyber-physical cascading failure and resilience of power grid: A comprehensive review. Frontiers in Energy Research, 11, 1095303. https://doi.org/10.3389/fenrg.2023.1095303.

International Journal of Electrical and Electronics Research (IJEER)
Research Article | Volume 14, Issue 1| Pages 73-85|e-ISSN: 2347-470X

[4] Amiri, M. H. N., Fotuhi-Firuzabad, M., & Moeini-Aghtaie, M. (2024). Towards a framework for measurements of power systems resilience. Sustainable Energy, Grids and Networks, 40, 101325. https://doi.org/10.1016/j.segan.2024.101325

[5] Zhou, S., et al. (2023). Enhancing the resilience of the power system to high-penetration renewable and intelligent control environments. Frontiers in Energy Research, 11, 1256850. https://doi.org/10.3389/fenrg.2023.1256850.

[6] Su, Q., Zhang, H., & Wang, T. (2024). A new model of electrical cyber–physical systems with stochastic communication link failures. ISA Transactions, 137, 98–112. https://doi.org/10.1016/j.isatra.2023.11.021

[7] Guo, X., Miao, G., Wang, X., Yuan, L., Ma, H., & Wang, B. (2023). Mobile energy storage system scheduling strategy for improving the resilience of distribution networks under ice disasters. Processes, 11(12), 3339. https://doi.org/10.3390/pr11123339

[8] Tightiz, L., & Yang, H. (2021). Resilience microgrid as power system integrity protection scheme element with reinforcement learning-based management. IEEE Access, 9, 83963–83975. https://doi.org/10.1109/ACCESS.2021.3087491

[9] Qin, Y., Liu, X., & Wang, L. (2023). Communication delay impacts on secondary frequency control of power systems: A robust design perspective. Electric Power Systems Research, 214, 108561. https://doi.org/10.1016/j.epsr.2023.108561

[10] Fang, X., & Liao, Y. (2023). Resilience enhancement in cyber–physical power systems using distributed model predictive control. International Journal of Electrical Power & Energy Systems, 150, 109054. https://doi.org/10.1016/j.ijepes.2023.109054

[11] Li, B., Zhang, W., & Zhao, J. (2022). Distribution system restoration with communication constraints: A resilience-oriented approach. Electric Power Systems Research, 211, 108306. https://doi.org/10.1016/j.epsr.2022.108306

[12] Yang, R., & Li, Y. (2024). Operator cognitive load and decision latency under cascading power system events. Cognitive Systems Research, 80, 102082. https://doi.org/10.1016/j.cogsys.2023.102082

[13] Huang, H., Liu, D., & Zhang, W. (2024). Reinforcement learning-based resilient voltage control for cyber-physical power systems. IEEE Transactions on Smart Grid, 15(2), 1887–1898. https://doi.org/10.1109/TSG.2023.3331298

[14] Abdelrahman, M. S., Kadry, S., & Shafiee, K. (2024). Digital-twin-driven cyber-physical resilience of microgrid control using AI-based analytics. Energies, 17(16), 3927. https://doi.org/10.3390/en17163927

[15] Li, P., Xu, Y., & Dong, Z. Y. (2023). Federated reinforcement learning for distributed voltage regulation in power grids. IEEE Transactions on Power Systems, 38(6), 5430–5441. https://doi.org/10.1109/TPWRS.2023.3258710

[16] Kim, S., Choi, J., & Lee, D. (2023). Deep learning-assisted anomaly detection for smart-grid communication networks. Electric Power Systems Research, 218, 109148. https://doi.org/10.1016/j.epsr.2023.109148

[17] Zhang, H., Guo, X., & Wang, Y. (2022). Adaptive model predictive control for resilient microgrids under cyber-attack and communication delay. International Journal of Electrical Power & Energy Systems, 143, 108420. https://doi.org/10.1016/j.ijepes.2022.108420

[18] Zhang, C., & Amin, M. (2021). Human-in-the-loop power-system resilience: Concepts and challenges. IEEE Access, 9, 117500–117515. https://doi.org/10.1109/ACCESS.2021.3107278

[19] Li, Y., & Wu, Q. (2022). Modeling human decision latency and its impact on dynamic security of power systems. International Journal of Electrical Power & Energy Systems, 136, 107661. https://doi.org/10.1016/j.ijepes.2021.107661

[20] Xie, S., Wang, K., & Li, Z. (2023). Cognitive digital-twin modeling for operator-in-the-loop control in smart-grid environments. Applied Energy, 344, 121217. https://doi.org/10.1016/j.apenergy.2023.121217

[21] Peters, K., & Chen, M. (2024). Human-factor-aware reinforcement learning for grid resilience under uncertainty. IEEE Transactions on Neural Networks and Learning Systems, 35(9), 10412–10425. https://doi.org/10.1109/TNNLS.2023.3272914

[22] Dobson, I., Carreras, B. A., & Newman, D. E. (2021). A branching process approximation to cascading blackout risk. IEEE Transactions on Power Systems, 36(4), 3535–3545. https://doi.org/10.1109/TPWRS.2020.3048823

[23] Liu, X., Liu, J., Zhang, W., & Ma, K. (2024). Impact of communication-link overload on cascading failure in cyber-physical power systems. Electronics, 13(15), 3065. https://doi.org/10.3390/electronics13153065

[24] Ouyang, M. (2021). Review on modeling and simulation of interdependent critical infrastructure systems. Reliability Engineering & System Safety, 214, 107627. https://doi.org/10.1016/j.ress.2021.107627

[25] Li, S., Liu, T., & Zhang, J. (2022). Cascading failure vulnerability analysis of cyber-physical power grids under intentional attacks. Complexity, 2022, 8820413. https://doi.org/10.1155/2022/8820413

[26] Wang, Z., Chen, C., & Wang, J. (2020). Networked microgrids for grid resilience: A review. IEEE Transactions on Smart Grid, 11(6), 6105–6123. https://doi.org/10.1109/TSG.2020.3010570

[27] Panteli, M., & Mancarella, P. (2020). Influence of extreme weather and climate change on the resilience of power systems: A global perspective. IEEE Transactions on Power Systems, 35(5), 3992–4002. https://doi.org/10.1109/TPWRS.2020.2968436

[28] Hines, P., Dobson, I., Carreras, B. A., & Newman, D. E. (2020). Cascading power outages propagate locally in an influence graph that is not the actual grid topology. IEEE Transactions on Power Systems, 35(6), 5121–5131. https://doi.org/10.1109/TPWRS.2020.3001776

[29] Mishra, D. K., Ghosh, S., & Sinha, A. K. (2024). A detailed review of power system resilience enhancement pillars. Electric Power Systems Research, 229, 109880. https://doi.org/10.1016/j.epsr.2024.109880

[30] Li, Z., & Shahidehpour, M. (2021). Resilience of distribution systems with microgrids: A review. Electric Power Systems Research, 196, 107198. https://doi.org/10.1016/j.epsr.2021.107198

[31] Yan, R., Saha, T. K., & Chu, Y. (2021). Grid-edge visibility and resilience with PMUs. IEEE Transactions on Smart Grid, 12(2), 1185–1196. https://doi.org/10.1109/TSG.2020.3029841

[32] Rahimi, F., & Ipakchi, A. (2020). Using distributed energy resources to enhance grid resilience. IEEE Power & Energy Magazine, 18(4), 72–82. https://doi.org/10.1109/MPE.2020.2997916

[33] Gholami, A., Shekari, T., & Mohsenian-Rad, H. (2020). Microgrid resilience: A comprehensive review on protection strategies. IEEE Transactions on Smart Grid, 11(5), 4555–4570. https://doi.org/10.1109/TSG.2020.2995786

[34] Wang, Q., Zhou, M., & Chiang, H.-D. (2022). Cascading failure risk assessment using influence graphs and machine learning. IEEE Access, 10, 52301–52312. https://doi.org/10.1109/ACCESS.2022.3170935

[35] Zhang, Y., Wang, J., & Chen, C. (2021). Resilience-oriented distribution system planning with traffic-constrained repair crews and mobile power sources. IEEE Transactions on Power Systems, 36(2), 1473–1485. https://doi.org/10.1109/TPWRS.2020.3019574

[36] Panteli, M., Trakas, D. N., Mancarella, P., & Hatziargyriou, N. D. (2020). Metrics and quantification of operational resilience in power systems. IEEE Transactions on Power Systems, 35(3), 2256–2266. https://doi.org/10.1109/TPWRS.2019.2954659

International Journal of
Electrical and Electronics Research (IJEER)
Research Article | Volume 14, Issue 1| Pages 73-85|e-ISSN: 2347-470X

[37] Liu, Z., Ding, T., & Shahidehpour, M. (2021). Resilient distribution system planning with microgrids and mobile energy storage. IEEE Transactions on Smart Grid, 12(1), 25–37. https://doi.org/10.1109/TSG.2020.3013864

[38] Li, M., Zhang, Y., & Wang, J. (2022). Cyber–physical power system resilience: A survey. International Journal of Critical Infrastructure Protection, 37, 100507. https://doi.org/10.1016/j.ijcip.2022.100507

[39] Yan, R., Saha, T. K., & Masood, N. (2020). Impact of communication failures on protection and control in modern distribution networks. International Journal of Electrical Power & Energy Systems, 121, 106046. https://doi.org/10.1016/j.ijepes.2020.106046

[40] Wang, J., Chen, C., & Baldick, R. (2020). Research on resilience of interdependent critical infrastructures. IEEE Transactions on Smart Grid, 11(4), 3557–3570. https://doi.org/10.1109/TSG.2019.2957960.